Practical Model-Based Methodologies to Determine the State of Charge of Li/CFx Batteries

BY

EUGENE LEE

B.S., University of California, Berkeley, 2008

THESIS

Submitted as partial fulfillment of the requirements

for the degree of Master of Science in Materials Engineering

in the Graduate College of the University of Illinois at Chicago, 2016

Chicago, Illinois

Defense Committee:

Eduard Karpov, Chair and Advisor, CME

Michael J. McNallan, CME

Didem Ozevin, CME

Acknowledgements

Countless thanks must be given to my advisor Professor Eduard Karpov for his continuous support and boundless patience. Thank you for offering your time and expertise, and thank you for providing me with the opportunity to succeed.

I must also thank my committee members Professors Didem Ozevin and Michael J. McNallan for taking time out of their busy schedules to provide advice and guidance.

Finally, I express my deepest thanks to my friends and family, whose unwavering love and encouragement has allowed me to come this far.

TABLE OF CONTENTS

LIST OF TABLES

LIST OF FIGURES

SUMMARY

In the realm of primary cells, the Li/CF_x chemistry holds immense potential due to its unmatched theoretical specific energy, longevity, and shelf time. However, little work has been done on creating a simple, practical methodology to determine the state of charge (SoC) of a partially-discharged battery in critical applications, such as remote sensing and probing, and mission control hardware. We propose an approach in which the SoC can be estimated by measuring the output voltage under various current loads and fitting the data to an original model in the general form of a logistic curve. The resulting function can then be used in conjunction with least squares analysis to efficiently estimate the SoC.

1 INTRODUCTION

Much of current chemical energy storage research is focused on secondary batteries due to the ever increasing popularity of portable electronic devices[1, 13, 17, 19, 38, 41], electric vehicles[7, 8, 37], and large-scale energy storage systems[12, 34]. On the other hand, primary batteries still play crucial roles in many industrial segments, most notably in the the medical and military sectors[6, 32, 36]. Primary batteries offer cheaper, high power, high energy density alternatives when charging is either impossible or unnecessary, as in the cases of medical implants, autonomous defense systems, and deep space probes. Lithium cells in particular have become preferred for such specialized industries due to their high energy density[6, 18, 22], and of the variety of available cathode chemistries, CF_x has generated great interest owing to its particularly high theoretical specific capacity[24, 29, 30, 31, 40, 41]. Though CF_x performs less effectivley at higher discharge rates and low temperatures[24], its potential remains unmatched for applications that have a low power demand and operate in moderate environments for very extended periods of time.

Due to the critical nature of the aforementioned applications, it is of vital importance to be able to quickly and simply determine the state of charge and remaining lifetime of primary batteries. Various analytical techniques have been proposed for secondary batteries, ranging from using extended Kalman filters[20, 16] and fuzzy neural networks[21] to more straightforward Coulomb counting[10, 28], but little literature has been published on state of charge measurements for primary cells. Determining the remaining charge in batteries with CF_x cathodes in particular has proven to be difficult because the discharge curve is essentially

flat[30, 40, 39], meaning that there is little voltage variation throughout the discharge process. In this thesis, we propose such a methodology based on a nonlinear fit to the measured voltage data taken for a reference cell at various applied currents. These sigmoidal fits can then be used as reference curves to which an arbitrary cell with similar specifications can be compared and evaluated using the least squares technique.

2 BACKGROUND

Commercial primary lithium batteries largely use lithium metal as the anode due to its low molar weight, high specific capacity, and the fact that it is the most electropositive alkali metal[18, 31]. Thus the variety of chemistries we will review below are exclusively cathode chemistries. It should also be noted that all stated specific capacities are theoretical capacities as a result of the difficultly inherent in assessing the practical capacities of cathodes produced using different methodologies and in varying environments. Practical capacities are significantly less than the given theoretical figures, though the relative rankings remain the same.

2.1 Primary Lithium Battery Chemistries

2.1.1 Manganese Dioxide, MnO_2

Electrolytic manganese dioxide (EMD) is the most common primary lithium cathode chemistry on the market, constituting roughly 80% of all commercially sold primary lithium cells[18]. It occurs as a wide variety of polymorphs, including α-MnO_2 (often referred to as hollandite), β-MnO_2 (often referred to as pyrolusite), and γ-MnO_2[9]. The γ-phase is what is largely utilized in the production of primary lithium batteries, and has a complex structure that can be described as ramsdellite interspersed with rutile-like pyrolusite with microtwinning defects throughout the crystal. Alternately, the structure can be described as "tunnels" of space defined by rows of octahedral units of MnO_6 (Fig. 1), broken up into aligned chunks by microtwinning defects.

The result is a chemistry that has a theoretical specific energy of around 310 mAh/g, the

capability to be used for both high and low drain applications, good safety, and relatively low cost [18, 31]. Due to its numerous positive characteristics, MnO_2 batteries have are used in a wide variety of circumstances ranging from digital cameras and calculators to small military electronics[31].

$$Li + Mn^{IV}O_2 \rightarrow LiMn^{III}O_2 \tag{1}$$

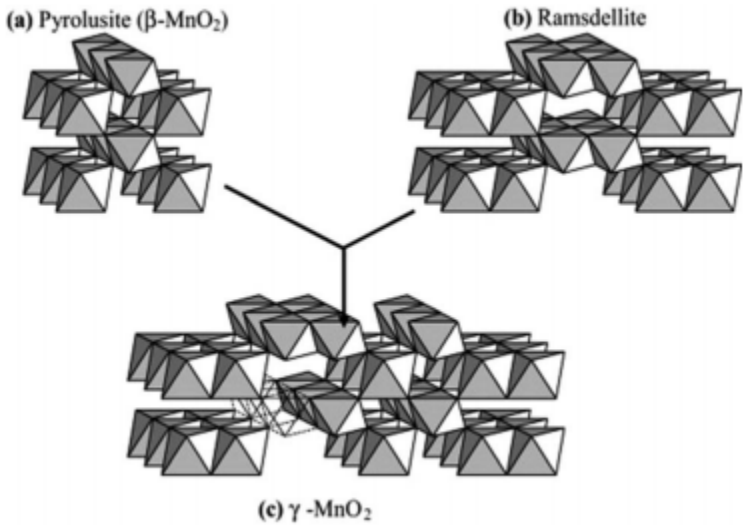

Figure 1: Depiction of γ-MnO_2 structure, with ramsdellite and pyrolusite structures for reference. Reproduced from Ref. [5] with permission from The Royal Society of Chemistry

2.1.2 Silver Vanadium Oxide (SVO), $Ag_2V_4O_{11}$

The SVO chemistry was developed relatively recently, and was first used in a medical implant in 1987. SVO batteries are in fact utilized almost exclusively for implantable cardioverter defibrillators (ICD) due to their ability to deliver high currents while having low self-discharge rates. The ability to discharge rapidly allows the battery to quickly charge the capacitor in an

ICD so that it can deliver a pulse of energy up to 35 J[4]. This capability is attributable to the silver atoms intercalated in the vanadium-oxygen layers, creating a C-centered monoclinic unit cell[18]. These atoms reduce to metallic silver during discharge and considerably raise the conductivity of the material as a whole[6, 31].

$$7\mathrm{Li} + \mathrm{Ag_2V_4O_{11}} \rightarrow \mathrm{Li_7Ag_2V_4O_{11}} \tag{2}$$

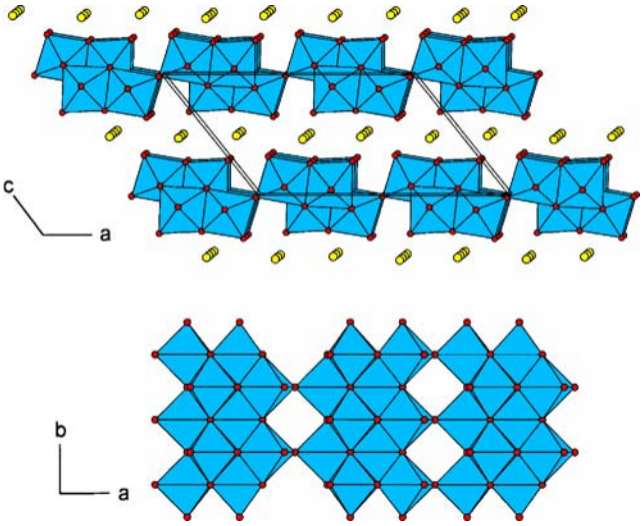

Figure 2: Depiction of ε-$\mathrm{Ag_2V_4O_{11}}$ structure. Silver atoms are colored yellow, oxygen atoms are colored red. Vanadium atoms are located at the center of the octahedra. Reproduced from Ref. [4] with permission from Springer

SVO has a theoretical specific capacity of around 315 mAh/g[6, 35], making it quite competitive with with manganese dioxide, but displays a unique two-plateau discharging profile. When an SVO cell is discharged under constant load, a film forms on the lithium anode and eventually increases the internal resistance of the system, effectively decreasing the nominal cell voltage and introducing a voltage delay[6, 18, 31]. This is helpful when identifying the

state of charge of the battery, but makes extended use of the battery more difficult, and has led researchers to attempt to combine SVO with CF_x to create a material with the best characteristics of both chemistries.

2.1.3 Polycarbon Monofluoride, $(\mathbf{CF}_x)_\mathbf{n}$

Also referred to as graphite fluoride, the CF_x structure can be described as fluorinated sheets of graphene, with the value of x usually ranging between 0.9 and 1.2. It is a gray, thermally stable powder that is synthesized by reacting fluorine gas with a relatively pure carbon compound at high temperatures[14, 27]. The carbon compound is often petroleum coke or graphite, but different forms of carbon feedstocks such as carbon black can also be used[14, 27, 31]. The chemistry's greatest advantage lies in its immense theoretical specific capacity of 860 mAh/g (partially due to its low density), and though practical applications result in an actual capacity of 400 mAh/g[18], CF_x remains one of the most energy-dense materials available. This explains the continued interest and research into CF_x, since the remaining untapped potential is significant. The material also exhibits very low self-discharge rates of 0.5% to 1.0% per year as well as excellent safety characteristics[24]. The reason behind the lack of danger is that it has relatively poor electrical conductivity, though it should be noted that as the cell continues to discharge, the graphite becomes defluorinated and gradually gains conductivity[31]. Despite this drawback, carbon monofluoride's properties have led to the cathodes being used in a wide variety of low-power, long-life applications such as pacemakers, portable electronics, utility meters, and military technologies such as communications equipment[31].

$$nx\text{Li} + (\text{CF}_x)_n \rightarrow nx\text{LiF} + n\text{C} \tag{3}$$

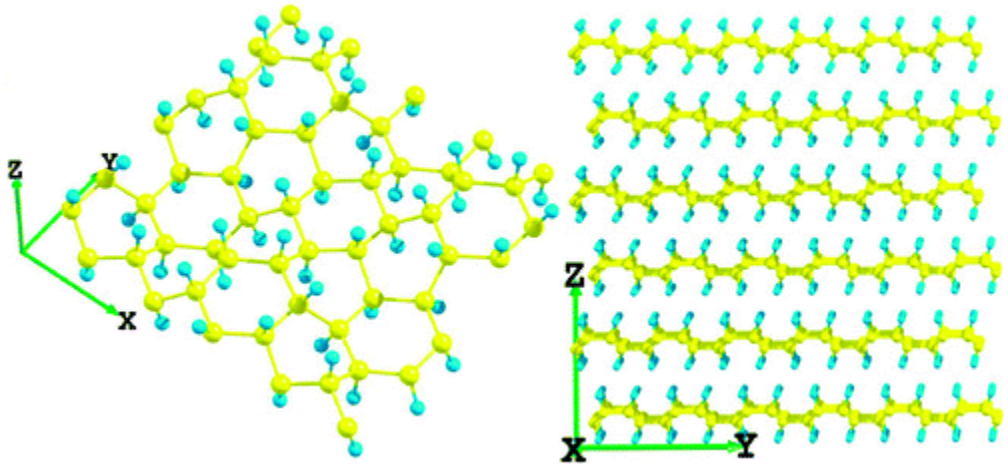

Figure 3: Depiction of CF_x structure. Carbon atoms are colored yellow, fluorine atoms are colored cyan. Reprinted with permission from [2]. Copyright 2010 American Chemical Society.

This wide-ranging applicability is only possible due to the equally diverse geometries in which CF_x can be produced, including coins, cylinders, and pins. Like the previously mentioned chemistries, cells are largely constructed with an elemental lithium anode, an electrolyte which is a mix of a lithiated salt such as $LiBF_4$ or $LiPF_6$ and an organic solvent such as ethylene carbonate or γ-butyrolactone, and a separator[14, 18, 31]. As long as the electrode materials are structurally supported - either by being attached to a stronger material (as in the case of a current collector in a cylindrical cell) or by virtue of the inherent form (as in a coin cell) - the cell can be constructed in virtually any shape desired. The result is that most companies offer the option of customized packaging.

CF_x does however have a significant disadvantage in the form of its particularly flat dis-

charge curve. Unlike an SVO cell which is marked by the sudden increase in internal resistance, a CF_x cell that is discharged under a constant load displays a very consistent measured voltage that only drops rapidly at a very high depth of discharge. As these are primary batteries, the determination of their state of charge is not a trivial problem since they are not designed to be recharged. Significant work has been done to solve this issue, some of which are presented in the next section.

2.2 State of Charge Estimation Methods

The importance of estimating the state of charge of a battery quickly and accurately is clear, especially if it is being used in a critical application such as a medical implant. Current available techniques can generally be separated into one of three categories: book-keeping, adaptive systems, or direct measurement[10]. Though there is a large (and increasing) number of available methodologies, only three of the most commonly studied and used ones will be reviewed here for the sake of brevity.

2.2.1 Coulomb Counting

Coulomb counting is a book-keeping method in which the remaining charge is determined by calculating how much charge has left the system. This is done by measuring the discharge current and integrating over the time of discharge, resulting in a nearly literal count of number of electrons transferred from the anode to the cathode[3, 10, 25, 28]. Despite this method's inherent simplicity, there are various sources of inaccuracy that must be accounted for, including self-discharge losses, actual maximum capacity determination, and temperature and discharge

rate-dependent discharge efficiency. Depending on the materials in the cell, the ambient temperature, and the current state of charge, self-discharge losses can be notable, and since the mechanism behind self-discharge does not involve the flow of charge between terminals, it must be considered separately from the rest of the counting system[3, 28]. The maximum capacity of the cell is also likely to be different from the nominal capacity as a consequence of varying manufacturing environments and slight differences in the materials themselves. Finally, the system must also account for the battery discharging efficiency, which describes how much of the contained charge can actually be accessed[3, 10, 28]. This is determined by the reaction kinetics of the cell, which in turn implies that the efficiency is dependent on both ambient temperature as well as discharge rate. There is no standardized solution to incorporate the effiiciency into the coulomb counting method, so custom calculation modifications must be made on a cell-by-cell basis.

2.2.2 Kalman Filter

The Kalman filter is an algorithm which predicts the future state of a system based on data collected from the current state of the system. To clarify, it is a recursive method that combines the predicted data with the current data to produce another more accurate estimate of future data[10, 11, 15, 16]. This concept can be compactly stated as follows:

$$\mathbf{x}_n = \mathbf{A}_{n-1,n}\mathbf{x}_{n-1} + \mathbf{w}_n \tag{4}$$

$$\mathbf{y}_n = \mathbf{C}_n\mathbf{x}_n + \mathbf{v}_n \tag{5}$$

Eqn. 4 is the state equation, where $\mathbf{x}_n$ is the actual state of the system at time n, $\mathbf{A}$ is the state transition matrix from $n-1$ to n, and $\mathbf{w}_n$ is a zero mean white noise vector. Eqn. 5 is the observation equation, where $\mathbf{y}_n$ is the observed vector, $\mathbf{C}_n$ is the measurement matrix, and $\mathbf{v}_n$ is a zero mean white noise vector that is independent from $\mathbf{w}_n$[15]. The state equation can more simply be described as stating that when some matrix $\mathbf{A}$ operates on the state vector at time $n-1$ and this quantity is summed with some amount of randomized noise, the result is the state vector at time n. The observation equation can also be described textually by stating that the observation vector $\mathbf{y}$ at time n is equivalent to the components of the state vector which are being measured, with each component summed with some amount of randomized noise. In practice, the actual state of the system is not known, so Eqn. 6 is used to find an estimated state vector.

$$\hat{\mathbf{x}}_{n,n} = \hat{\mathbf{x}}_{n,n-1} + \mathbf{K}_n\left(\mathbf{y}_n - \mathbf{C}_n\hat{\mathbf{x}}_{n,n-1}\right) \tag{6}$$

The matrix $\mathbf{K}$ is the Kalman gain, and can be calculated from the covariance matrices of the previous state vector and the two white noise vectors. As this is not a thesis describing the Kalman filter method, the specifics of the calculation process will be avoided.

Most of the methods developed for determining the SoC use the extended Kalman filter, which is a nonlinear extension of the Kalman filter. This naturally lends itself to use in bat-

tery systems since the internal mechanisms that drive the cells are inherently nonlinear (e.g. diffusion). The fundamental concept remains the same however, with commonly measured properties being voltage, discharge current, internal resistance, and temperature[11]. The resulting SoC estimates have been shown to have accuracies within 1%[11], making the Kalman filter one of the best choices for applications requiring a high degree of accuracy. However, there are two major disadvantages. First, much time must be expended in ensuring that the chosen model is appropriate and applicable to the system at hand. Second, depending on the number of measurements and variables, the required computing power can be significant.

2.2.3 Electrochemical Impedance Spectroscopy

Electrochemical impedance spectroscopy (EIS) is a direct measurement method that infers information about the state of an electrochemical system by measuring the impedance of the system over a wide range of AC frequencies[10, 28, 31, 33]. Before delving into the technique itself, some background information and terminology will be covered for the sake of clarification.

Impedance is effectively a generalized form of resistance which measures not only a circuit element's opposition to a static current but also to a current changing with respect to time. This is mathematically expressed as $Z = R + iX$, where the impedance Z is a sum of the static resistance R and the dynamic resistance X. X, called the reactance, is imaginary by virtue of its relation to oscillating functions. Thus elements such as capacitors and inductors can also be given impedance values, which in the ideal case are purely imaginary. Impedances

are a function of frequency, and can therefore be parametrically visualized in what are called 'Nyquist plots' by using the imaginary component and real component of the impedance evaluated at each frequency as coordinates on the plot.

Electrochemical cells are often approximated by an equivalent electrical circuit called a Randles circuit (Fig. 4). The electrolyte solution and the electron-transfer process are both modeled as straightforward resistors, but the other two elements are more complex. The electrical double layer is a concept in which a charged surface - in this case, an electrode - causes ions of the opposite charge to be adsorbed onto the surface, which in turn causes a loosely organized layer of mixed-charge ions to form in response, with a greater emphasis on ions with the charge of the electrode[23]. These two layers act like the plates in a traditional capacitor, which then means that when the system is subjected to an oscillating potential, the double layer also contributes impedance to the currently flow. However, since the double layer is not a static structure, modeling its contribution as a simple capacitor is not entirely accurate, and as such it is sometimes replaced by what is called a constant phase element to represent an imperfect capacitor[31]. The Warburg element exists in case the diffusion process at the electrode-electrolyte interface is a limiting process, and is therefore placed in series with the charge-transfer resistor.

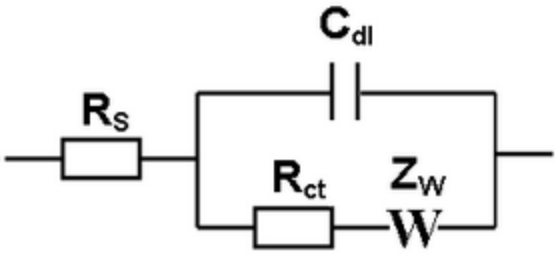

Figure 4: The Randles circuit. R_S is the electrolyte solution resistance, R_{ct} is the charge-transfer resistance, C_{dl} is the electrical double layer capacitance, Z_W is a Warburg impedance element

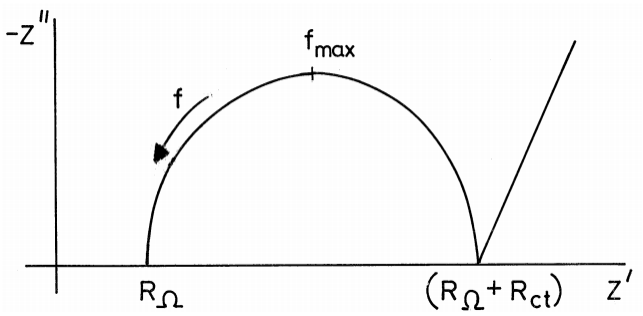

Figure 5: Generalized Nyquist plot of the circuit from Fig. 4, where R_Ω is the equivalent of R_S. Reproduced from Ref. [33] with permission from Elsevier

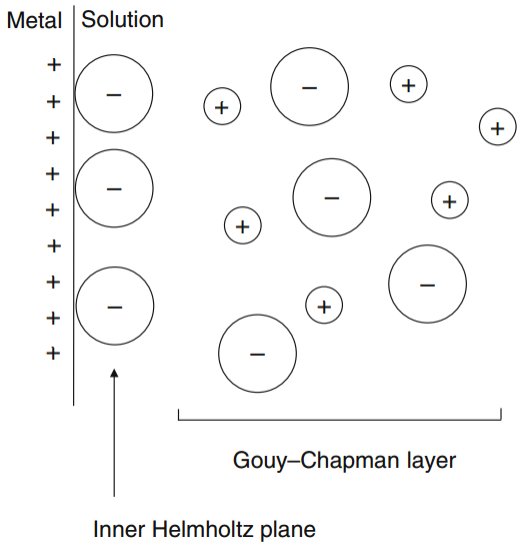

Figure 6: Depiction of the electrical double layer at a metal-solution interface. Reproduced from Ref. [23] with permission from Springer

Assuming that a reasonable equivalent electric circuit is chosen, any electrochemical cell's impedance can be defined as a function of frequency. This analysis method is known as EIS. As a cell discharges, this function evolves over time in a fashion unique to each chemistry, and this change can theoretically be used to determine the SoC of the cell[10, 33]. The difficulties inherent in this process are numerous: it is very temperature dependent, requires much computational power, and demands an accurate circuit model of the system. As such, EIS is rarely used in practice as a SoC estimation technique[26]. Our proposed methodology is a direct measurement method that avoids the computational difficulties that EIS poses and provides a framework for quickly and simply determining a practical model for a primary cell.

3 EXPERIMENTAL PROCEDURE

3.1 Equipment

A circuit was constructed to measure voltages and discharge times of BR2325 coin cells as an example of a specific CF_x cell of interest(1) (Fig. 9). A galvanostat(2) was used to maintain a constant current through the circuit, while data was collected using a ADC-24 Data Logger(3) from Pico Technology Ltd. Two different galvanostats were used over the course of data collection: a Keithley SourceMeter 2400 and a Xantrex XDL 35-5P. The experimental setup was designed with a variable resistor(4) (in the form of a resistance substitution box from IET Labs) so as to keep the system's overall potential drop similar between tests with different current loads. Additionally, two 20 kΩ resistors were used to keep the measured voltage within the data logger's specifications.

Figure 7: Keithley SourceMeter®2400 Galvanostat

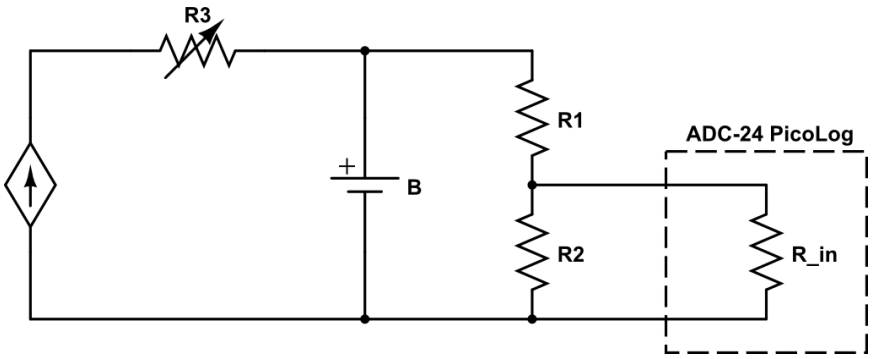

Figure 8: Diagram of the circuit used for data collection; R_{in} is the internal resistance of the measurement device, and B is the measured battery

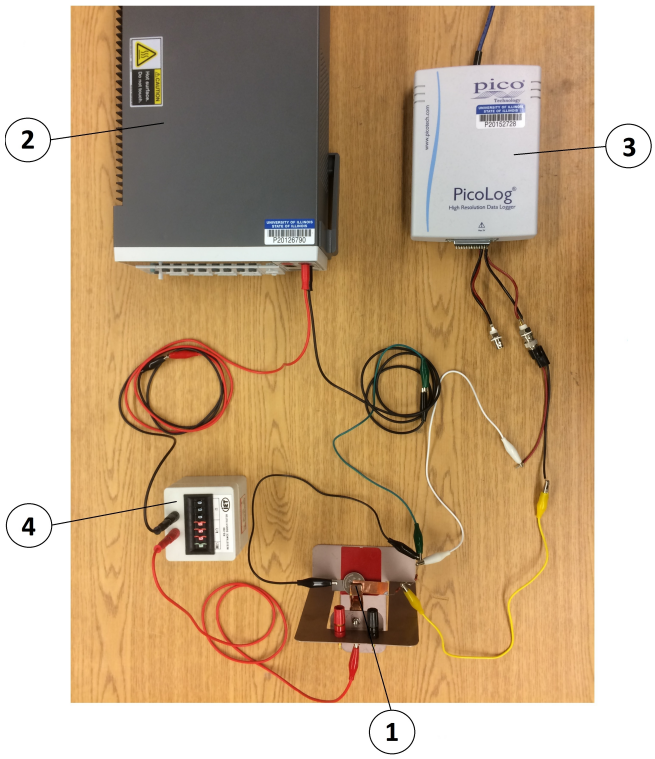

Figure 9: Physical setup used for data collection: 1) Cell of interest, 2) galvanostat, 3) data logger, 4) esistance substitution box

3.2 Experimental Methods

3.2.1 Data Collection

The Keithley 2400 SourceMeter was used to collect the measured voltage data for the 0.1 mA test, and the Xantrex XDL 35-5P was used for the 0.3 mA, 1.0 mA, 3.2 mA, 10 mA, and 32 mA tests, for a total of six data sets (Fig. 10). Additionally, the SourceMeter was used to perform voltage sweeps on new cells to validate both the short-circuit current and open-circuit voltage values (inset Fig. 11).

3.2.2 Data Processing

The data was then processed to convert the time stamps to depth of discharge values (θ) by dividing each set's data points by the respective total run time of reaching a zero cell voltage. New data sets were then constructed from the data, grouped by discrete θ values (Table 1). Since the discharge profile of CF_x cells tends to be very flat during the initial period of discharge, a greater number of sets were taken from higher theta values since they provided better differentiation.

3.2.3 Proposed Model

The measured voltage can be expected to approach an asymptote as the applied current approaches zero and decrease exponentially at higher currents. This led to the decision to fit the data to a sigmoid logistic function of the form seen in Eqn 7.

$$V\left(I,\theta\right)=2V_{OC}\left[-\frac{1}{2}+\frac{1}{1+e^{a(b+\ln I)}}\right] \tag{7}$$

This equation can be rearranged into the form seen in Eqn. 8, where I_0 is a θ-dependent indicator of the short circuit current, a is a θ-dependent measure of the curve's steepness, V_{OC} is the open circuit voltage parameter, and I is the applied current.

$$V\left(I,\theta\right)=2V_{OC}\left[-\frac{1}{2}+\frac{1}{1+e^{a(I+I_0)}}\right] \tag{8}$$

4 RESULTS AND DISCUSSION

4.1 Preliminary Assumptions

It was observed that there was very little difference in the measured short circuit current for both directions of the voltage sweep of a fully charged cell, so a trial value of 0.2 A was chosen for the short circuit current. This meant that in addition to the collected data (Table 1), we could add an additional point at 0.2 A and 0 V. Since the fit was not constrained to this point, it can be seen that the short circuit current (i.e. the X-intercept of the curve) is not identical for each curve.

The open circuit voltage was also chosen to be a fixed point. Though this is not a wholly accurate representation of the physical processes inside the cell, it is not a large approximation either due to the observation that as the current load becomes smaller, the measured voltage approaches the shape of a step function (Fig. 11). Additionally, the measured voltage's dependence on θ is inconsistent and therefore precarious, as can be seen from the varying profiles of the empirical data's curves. By averaging the values of the y-intercepts of the voltage sweep curves (Fig. 11, inset), we were able to determine the approximate value of $V_{OC} = 2.74$. Each set of voltage vs. θ data was fit to the model proposed in Eqn. 7, resulting in six sets of parameters, (Table 1).

Table 1: Parameter values for the logistic fits at $V_{OC} = 2.74$ V

	a	b
$\theta = 0.2$	0.854	1.592
$\theta = 0.4$	0.821	1.591
$\theta = 0.6$	0.762	1.590
$\theta = 0.7$	0.702	1.572
$\theta = 0.8$	0.655	1.632
$\theta = 0.9$	0.524	1.888

4.2 Initial Attempts

Before the results are presented, our initial attempts to find a SoC estimation method based on only measured voltage will be discussed because knowing why and how they failed were arguably as enlightening as finding the successful approach.

Our first approach was to find an analytical function for the theta-dependent open circuit voltage by extrapolating the discrete-θ fits to $I \to -\infty$. This was before our eventual decision to fix the open circuit voltage, and we believed that finding this function was the way to achieve the highest accuracy. We were able to fit those six points and find the function, but we realized that this method was too easily skewed by the uncertainty of the small θ measurements. Additionally, the resulting function was so flat at lower values of θ that the error margins were far too small to be practical.

Even after deciding upon an approximate fixed open circuit voltage, developing Eqn. 7 still required careful consideration of the objectives of this study. Namely, the six data sets could be fit much more closely with a greater number of parameters, but this was misleading for a few reasons: first, the accuracy of the overall method would not necessarily follow from a fit with a lower error. Second, a large number of parameters would decrease the simplicity

and ease of calculation of this methodology. Finally, limiting our model to two parameters allowed us to glean some physical meaning from the parameters themselves.

4.3 Finding the Complete Function

The parameters a and b were then themselves fit to two exponential fits. This allowed us to express the measured voltage as a function of applied current and the state of discharge, which can in turn be visualized as a 3D surface (Fig. 13). Therefore, given any drain current and measured voltage, we can determine the depth of discharge with Eq. 7, where

$$a = 0.81 + 1.086 \cdot 10^{-4} e^{8.917\theta}, \; b = 1.586 + 5.224 \cdot 10^{-9} e^{19.858\theta} \tag{9}$$

When the resulting complete function is evaluated at a specific current, it can be seen that the profile is very flat at low depth of discharge and approaches 0 V as the depth of discharge approaches 1 (Fig. 14).

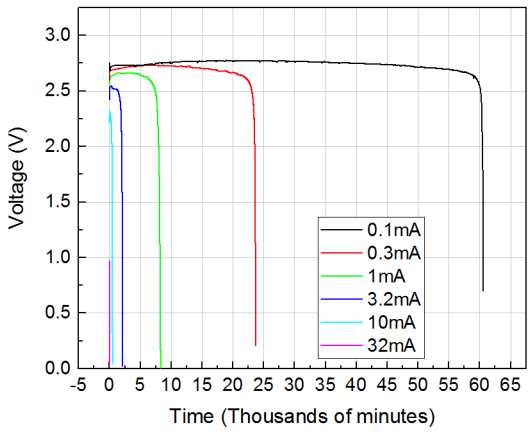

Figure 10: Initial collected data with six different load currents

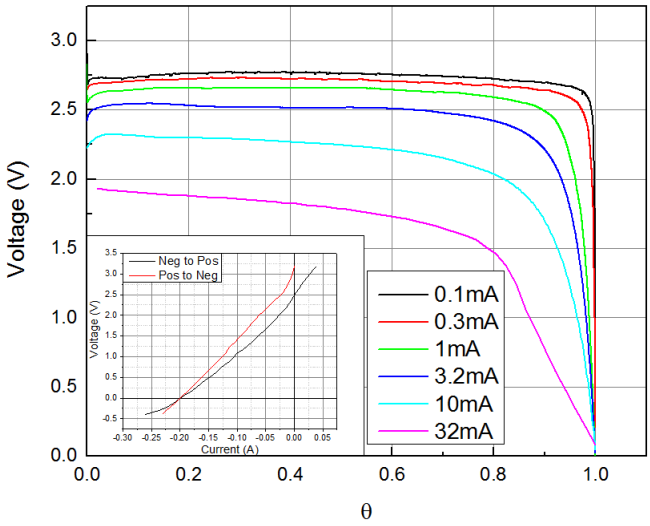

Figure 11: Initial collected data, with conversions from time to depth of discharge. Inset shows data from both forward and reverse voltage sweeps on a new cell

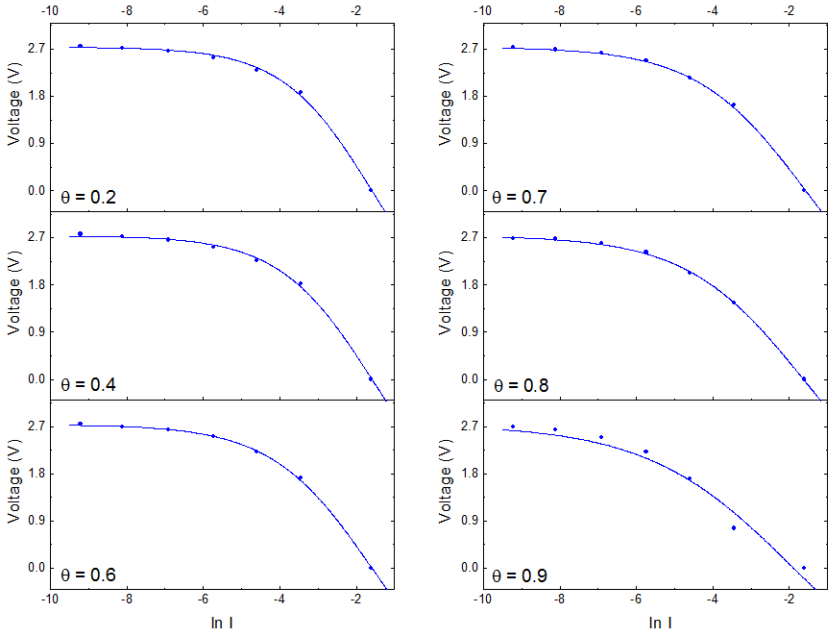

Figure 12: Plot of sigmoidal functions fit to the collected data, denoted by the circular markers. The markers at (ln 0.2, 0) denote the "trial" short circuit current

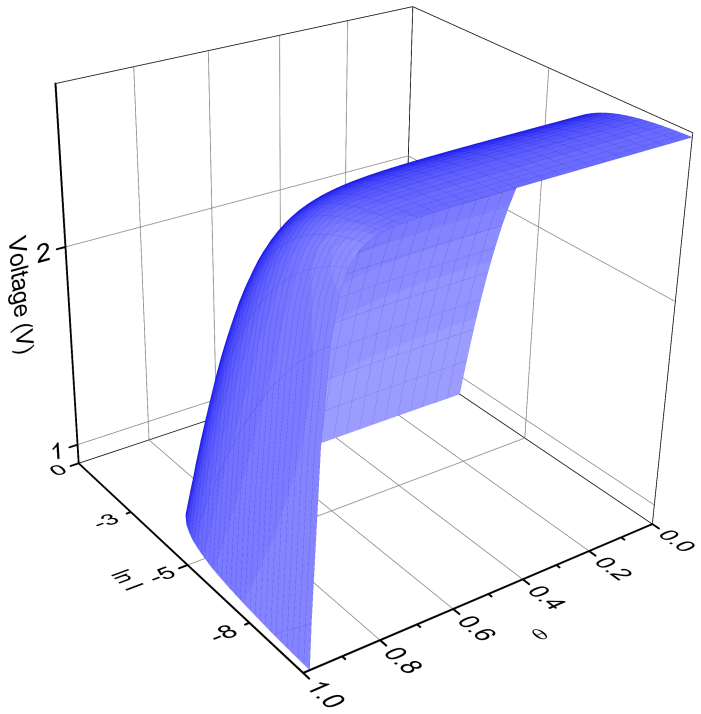

Figure 13: Surface plot of the measured voltage as a function of the natural logarithm of the applied current and the depth of discharge

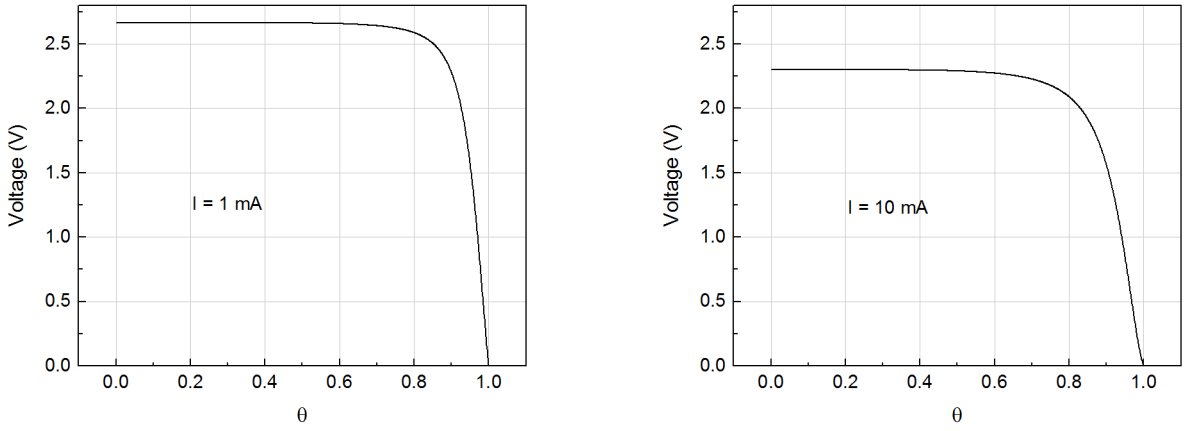

Figure 14: Cross section of the complete function at a) $I = 1$ mA and b) $I = 10$ mA

4.4 Application Example

Due to the possible variance in ambient conditions and the inherent differences between individual batteries[20], Eqn. 7 cannot serve as a universal function to determine θ. However, we can use the method of least squares to make an accurate estimate. If the voltage is measured at a particular applied current, we can define a residual as the difference between the measured voltage V_M and the expected voltage V_E. Repeating this process for multiple applied currents results in a set of residuals, which can then be squared and summed to provide a measure of the error. θ can then be found by minimizing the error.

$$Error = \sum_i r_i^2 = \sum_i \left[V_M - V_E\left(I_i, \theta\right)\right]^2 \tag{10}$$

As an example, here we demonstrate the processing of a set of simulated data taken from a battery at $\theta = 0.8$ under the aforementioned six different current loads. The six voltage-current data pairs results in six residuals, which are squared and summed to find the the total error (Eqn. 10). We then minimize the error by numerically solving for the θ at which the derivative of the error is zero, resulting in $\theta = 0.82$ (Fig. 15).

$$\begin{aligned} Error = &\left[1.41 - V_E\left(0.032, \theta\right)\right]^2 + \left[1.95 - V_E\left(0.01, \theta\right)\right]^2 + \\ &\left[2.35 - V_E\left(0.0032, \theta\right)\right]^2 + \left[2.63 - V_E\left(0.001, \theta\right)\right]^2 + \\ &\left[2.69 - V_E\left(3 \cdot 10^{-4}, \theta\right)\right]^2 + \left[2.73 - V_E\left(1 \cdot 10^{-4}, \theta\right)\right]^2 \end{aligned} \tag{11}$$

Table 2: Simulated measured voltage data for six different drain currents

Current (mA)	Voltage (V)
32	1.41
10	1.95
3.2	2.35
1.0	2.63
0.3	2.69
0.1	2.73

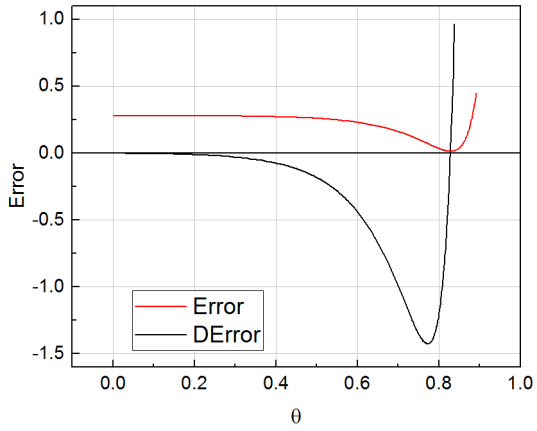

Figure 15: Plot of the derivative of the total error. The error is minimized at $\theta = 0.82$

4.5 Rescaling of the Method and Broader Usage

An important issue regarding the application of the proposed method is the testing of batteries with different capacities. If the size of the electrodes change, then one would expect that the testing current values would have to be rescaled. However, this can be done within the proposed model without having to take an entirely new series of tests with each battery. One possible approach is to employ a single fresh battery and determine six load currents I_i ($i = 1...6$) such that the five ratios of the corresponding measured voltages $\frac{V_{i+1}}{V_i}$ are the same as in the proposed model at $\theta \sim 0$ (i.e. calculated from Eqns. 7-9):

$$0.994035, 0.983377, 0.958748, 0.900327, 0.756785 \ (I_{i+1} > I_i) \tag{12}$$

These load currents are the new test currents that should be applied to the batteries of interest instead of the original current values mentioned in Fig. 10. Then one can take a partially discharged battery of interest, test it at these load currents and measure the corresponding voltages. The data set can then be run through the model in a manner similar to the one detailed previously, which will yield the θ for that battery.

The calculated voltages in Eqns. 7 or 8 could have been divided by V_{OC} to provide a dimensionless model, which would then familitate a more natural application of such a rescaling technique.

5 CONCLUSIONS

A methodology to quickly assess the state of charge of Li/CFx batteries was proposed. By taking voltage measurements of a battery at various applied currents and normalizing all data to the depth of discharge θ, we were able to construct fits for V vs $\ln I$ data sets at six discrete states of charge based on a logistic model. Each curve produced two parameters, and these parameters were then themselves fit, resulting in a single analytical expression for the measured voltage as a function of I and θ, which can be visualized as a surface. By using this function in conjunction with the least squares method, a polynomial function of theta results and an unknown Li/CF_x battery's state of charge can be numerically calculated. The means by which this method could be applied beyond the specific battery type tested in this thesis was also shown to be based on a choice of a particular set of load currents.

The major advantages conferred by this method are its low processing cost and flexibility. Since the reference model and parameters have already been calculated here, any implementation of this system would only have to numerically solve Eqn. 10. Furthermore, the use of the least squares method provides inherent flexibility to the technique that could partially account for unexpected variables.

It should be noted that further refinements of this methodology can certainly be made, particularly by increasing the number of benchmark tests, as well as taking into accout various environmental conditions. Even so, the proposed technique promises charge estimates at low costs and short testing times.

References

[1] Nurhaswani Alias and Ahmad Azmin Mohamad. Advances of aqueous rechargeable lithium-ion battery: A review. *Journal of Power Sources*, 274:237–251, 2015.

[2] Vasilii I. Artyukhov and Leonid A. Chernozatonskii. Structure and layer interaction in carbon monofluoride and graphane: A comparative computational study. *Journal of Physical Chemistry A*, 114(16):5389–5396, 2010.

[3] Yevgen Barsukov and Jinrong Qian. *Battery Power Management for Portable Devices*. Artech House, 2013.

[4] M. I. Bertoni, N. J. Kidner, T. O. Mason, T. a. Albrecht, E. M. Sorensen, and K. R. Poeppelmeier. Electrical and optical characterization of Ag2V4O11 and Ag4V2O6F2. *Journal of Electroceramics*, 18:189–195, 2007.

[5] A Biswal, B C Tripathy, K Sanjay, T Subbaiah, and M Minakshi. Electrolytic manganese dioxide (EMD): a perspective on worldwide production, reserves and its role in electrochemistry. *RSC Advances*, 5(72):58255–58283, 2015.

[6] David C. Bock, Amy C. Marschilok, Kenneth J. Takeuchi, and Esther S. Takeuchi. Batteries used to power implantable biomedical devices. *Electrochimica Acta*, 84:155–164, 2012.

[7] Andrew Burke. Batteries and Ultracapacitors for Electric, Hybrid, and Fuel Cell Vehicles. *Proceedings of the IEEE*, 95(4):806–820, 2007.

[8] E J Cairns and P Albertus. Batteries for Electric and Hybrid-Electric Vehicles. *Annual Review of Chemical and Biomolecular Engineering, Vol 1*, 1:299–320, 2010.

[9] Y. Chabre and J. Pannetier. Structural and electrochemical properties of the proton / γ-MnO2 system. *Progress in Solid State Chemistry*, 23(1):1–130, 1995.

[10] Wen-Yeau Chang. The State of Charge Estimating Methods for Battery : A Review. 2013(1), 2013.

[11] Zhihang Chen, Shiqi Qiu, M.Abul Masrur, and Yi Lu Murphey. Battery state of charge estimation based on a combined model of Extended Kalman Filter and neural networks. *The 2011 International Joint Conference on Neural Networks*, pages 2156–2163, 2011.

[12] B. Dunn, H. Kamath, and J.-M. Tarascon. Electrical Energy Storage for the Grid: A Battery of Choices. *Science*, 334(6058):928–935, 2011.

[13] Brian L. Ellis, Kyu Tae Lee, and Linda F. Nazar. Positive Electrode Materials for Li-Ion and Li-Batteries. *Chemistry of Materials*, 22(3):691–714, 2010.

[14] Wilson Greatbatch, C F Holmes, E S Takeuchi, and S J Ebel. Lithium / Carbon Monofluoride (Li / CFx): A New Pacemaker Battery. 19(November):1836–1841, 1996.

[15] Michael J. Grimble and Michael A. Johnson, editors. *Principles of Adaptive Filters and Self-learning Systems.* Advanced Textbooks in Control and Signal Processing. Springer-Verlag, London, 2005.

[16] Hongwen He, Rui Xiong, Xiaowei Zhang, Fengchun Sun, and JinXin Fan. State-of-charge estimation of the lithium-ion battery using an adaptive extended Kalman filter based on an improved Thevenin model. *Vehicular Technology, IEEE Transactions on*, 60(4):1461–1469, 2011.

[17] T Horiba. Lithium-Ion Battery Systems. *Proceedings of the IEEE*, 102(6):939–950, 2014.

[18] Christian Julien, Alain Mauger, Ashok Vijh, and Karim Zaghib. *Lithium Batteries*. Springer International Publishing, Cham, 2016.

[19] T. L. Kulova. New electrode materials for lithium-ion batteries (Review). *Russian Journal of Electrochemistry*, 49(1):1–25, 2013.

[20] Jaemoon Lee, Oanyong Nam, and B H Cho. Li-ion battery SOC estimation method based on the reduced order extended Kalman filtering. 174:9–15, 2007.

[21] I-Hsum Li, Wei-Yen Wang, Shun-Feng Su, and Yuang-Shung Lee. A merged fuzzy neural network and its applications in battery state-of-charge estimation. *IEEE Transactions on Energy Conversion*, 22(3):697–708, 2007.

[22] Diego Lisbona and Timothy Snee. A review of hazards associated with primary lithium and lithium-ion batteries. *Process Safety and Environmental Protection*, 89(6):434–442, 2011.

[23] E. McCafferty. Charged Interfaces. In *Introduction to Corrosion Science*, pages 33–56. Springer New York, New York, NY, 2010.

[24] Ganesan Nagasubramanian. Fabrication and Testing Capabilities for 18650 Li /(CF x) n Cells. 2:913–922, 2007.

[25] Kong Soon Ng, Chin Sien Moo, Yi Ping Chen, and Yao Ching Hsieh. Enhanced coulomb counting method for estimating state-of-charge and state-of-health of lithium-ion batteries. *Applied Energy*, 86(9):1506–1511, 2009.

[26] Sabine Piller, Marion Perrin, and Andreas Jossen. Methods for state-of-charge determination and their applications. *Journal of Power Sources*, 96(1):113–120, 2001.

[27] J P Pinheiro, M Dubois, Z Fawal, F Masin, R Yazami, and a Hamwi. Synthesis and Characterization of Highly Fluorinated Graphite Containing sp 2 and sp 3 Carbon. *Chemistry of Materials*, 16(9):1786–1792, 2004.

[28] Vipin Prajapati, Herbert Hess, Edward James William, Vishu Gupta, Matthew Huff, Milos Manic, Freeman Rufus, Ash Thakker, and Justin Govar. A literature review of state of-charge estimation techniques applicable to lithium poly-carbon monoflouride (LI/CFx) battery. *India International Conference on Power Electronics*, pages 1–8, 2011.

[29] Ezhiylmurugan Rangasamy, Juchuan Li, Gayatri Sahu, Nancy Dudney, and Chengdu Liang. Pushing the Theoretical Limit of Li-CF. 2014.

[30] Jeffrey Read, Evan Collins, Brandon Piekarski, and Sheng Zhang. LiF Formation and Cathode Swelling in the Li/CFx Battery. *Journal of The Electrochemical Society*, 158(5):A504, 2011.

[31] Thomas B. Reddy, editor. *Linden's Handbook of Batteries*. McGraw-Hill Education, 4th edition, 2011.

[32] Andrew Ritchie and Wilmont Howard. Recent developments and likely advances in lithium-ion batteries. *Journal of Power Sources*, 162(2):809–812, 2006.

[33] Shalini Rodrigues, N. Munichandraiah, and A. K. Shukla. Review of state-of-charge indication of batteries by means of a.c. impedance measurements. *Journal of Power Sources*, 87(1):12–20, 2000.

[34] Grigorii L. Soloveichik. Battery Technologies for Large-Scale Stationary Energy Storage. *Annual Review of Chemical and Biomolecular Engineering*, 2(1):503–527, jul 2011.

[35] Kenneth J. Takeuchi, Amy C. Marschilok, Steven M. Davis, Randolph A. Leising, and Esther S. Takeuchi. Silver vanadium oxides and related battery applications. *Coordination Chemistry Reviews*, 219-221:283–310, 2001.

[36] Colin A. Vincent. Lithium batteries: A 50-year perspective, 1959-2009. *Solid State Ionics*, 134(1-2):159–167, 2000.

[37] G. J. Wang, N. H. Zhao, L. C. Yang, Y. P. Wu, H. Q. Wu, and R. Holze. Characteristics of an aqueous rechargeable lithium battery (ARLB). *Electrochimica Acta*, 52:4911–4915, 2007.

[38] David L. Wood, Jianlin Li, and Claus Daniel. Prospects for reducing the processing cost of lithium ion batteries. *Journal of Power Sources*, 275:234–242, 2015.

[39] Q. Zhang, S. D'Astorg, P. Xiao, X. Zhang, and L. Lu. Carbon-coated fluorinated graphite for high energy and high power densities primary lithium batteries. *Journal of Power Sources*, 195:2914–2917, 2010.

[40] S S Zhang, D Foster, and J Read. A low temperature electrolyte for primary Li/CFx batteries. *Journal of Power Sources*, 188(2):532–537, 2009.

[41] Wei J. Zhang. A review of the electrochemical performance of alloy anodes for lithium-ion batteries. *Journal of Power Sources*, 196(1):13–24, 2011.

VITA

NAME: Eugene Lee

EDUCATION: B.S., Engineering Physics, University of California, Berkeley, Berkeley, 2008